

Continuous Detonation of a Mixture of Gaseous Hydrogen and Liquid Oxygen in a Plane–Radial Combustor with Exhaustion Toward the Periphery

F. A. Bykovskii^a, S. A. Zhdan^a, E. F. Vedernikov^a,
A. N. Samsonov^a, and E. L. Popov^a

UDC 534.222.2, 544.454.3

Published in *Fizika Goreniya i Vzryva*, Vol. 56, No. 6, pp. 69–77, November–December, 2020.
Original article submitted October 24, 2019; revision submitted February 19, 2020; accepted for publication February 19, 2020.

Abstract: Regimes of continuous spin detonation and continuous multifront detonation of a gas–droplet mixture of gaseous hydrogen and liquid oxygen in a plane–radial combustor (internal diameter of 100 mm and external diameter of 300 or 200 mm) with exhaustion toward the periphery are obtained for the first time. The detonation front height of the gas–droplet mixture is greater than that of the gas mixture, which is caused by the critical size of detonation existence. Centrifugal forces acting on the products behind the detonation wave front favor faster filling of the plane–radial combustor with the fresh mixture and increase the detonation front height.

Keywords: continuous spin detonation, continuous multifront detonation, gaseous hydrogen, liquid oxygen, transverse detonation waves, plane–radial combustor.

DOI: 10.1134/S0010508220060076

INTRODUCTION

By now, continuous spin detonation (CSD), continuous multifront detonation (CMD), and pulsed longitudinal detonation in plane–radial combustors with exhaustion toward the periphery has been studied only for gaseous fuel–oxygen mixtures, including those with hydrogen as a fuel [1–9]. However, the fuel components basically used in rocket engineering are liquid hydrogen and oxygen. As the critical state of hydrogen is reached at the temperature $T^* = 33.24$ K and pressure $p^* = 1.3$ MPa, while the critical state of oxygen is reached at $T^* = 154.78$ K and $p^* = 5.08$ MPa [10], hydrogen is usually injected into the combustor in the gaseous state, whereas oxygen may be in the gaseous or liquid state, depending on the conditions in the injection system and the pressure in the combustor. Experiments on detonation combustion of a mixture of hydrogen with liquid oxygen were previously performed in an annular cylindrical combustor [4].

The goal of the present study is to obtain and investigate the structure of detonation waves in flows of gaseous hydrogen and liquid oxygen in a plane–radial combustor with an internal diameter $d_{c1} = 100$ mm in the case of exhaustion toward the periphery.

1. ARRANGEMENT OF EXPERIMENTS

The experiments (see Fig. 1) were performed in the plane–radial combustor 1 with an internal diameter $d_{c1} = 100$ mm and exhaustion toward the periphery. The distance between the plane walls was $\Delta = 10$ mm, and the external diameter of the annular orifice through which the products exhausted was varied: $d_{c2} = 300$ or 200 mm. Thus, the combustor length was also varied: $L_c = (d_{c2} - d_{c1})/2$. A specific feature of the plane–radial combustor is that the distance between the plane walls is much smaller than the combustor diameter: $\Delta \ll d_{c1} < d_{c2}$. Some experiments were performed with uniform constriction of the channel toward the combustor exit, which ensured an approximately constant area of the circular cross section of the channel $S_\Delta \approx 31.4 \text{ cm}^2 = \text{const}$: from $\Delta = 10$ mm to

^aLavrent'ev Institute of Hydrodynamics, Siberian Branch,
Russian Academy of Sciences, Novosibirsk,
630090 Russia; bykovskii@hydro.nsc.ru.

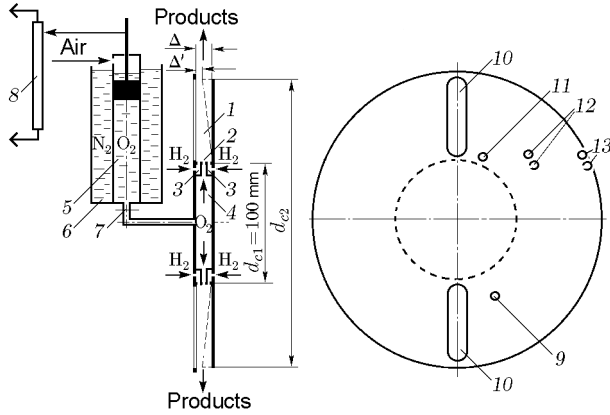


Fig. 1. Schematic of the plane-radial combustor with exhaustion toward the periphery.

$\Delta' = 3.3$ mm for $d_{c2} = 300$ mm and from $\Delta = 10$ mm to $\Delta' = 5$ mm for $d_{c2} = 200$ mm. In the case of a conical side wall, exact equality of the areas was provided only at the entrance and exit of the combustor channel. Inside the channel, the cross-sectional area first somewhat increased and then decreased. Separate injection of hydrogen and oxygen into the plane-radial combustor in the direction toward the periphery was performed through orifices 2 uniformly distributed over the circumference on the cylindrical wall and creating a system of colliding jets, which ensured mixing of the components near this wall. The total cross-sectional area of the orifices was $S_f = 45.6$ mm² for hydrogen and $S_{ox} = 30.4$ mm² for oxygen. Hydrogen was injected into the plane-radial combustor from a receiver with the volume $V_{r,f} = 13.5$ liters through manifolds 3, and oxygen was injected through a manifold 4 from the flowmeter 5 owing to displacement by a piston driven by the pressure of air located in the receiver with the volume $V_{r,a} = 4.2$ liters (the receivers are not shown in the figure). To prevent oxygen boiling, the flowmeter was located in a vessel filled by liquid nitrogen 6, and the piston was submerged into oxygen. Liquid oxygen was separated from the combustor by a diaphragm 7 made of thin aluminum foil. The initial pressures in the receivers were $p_{r,f0} = 55 \cdot 10^5$ Pa for hydrogen and $p_{r,ox0} = (22-50) \cdot 10^5$ Pa for air. The initial flow rate of hydrogen was $G_{f0} = 0.11$ kg/s, and the flow rate of oxygen was varied in the interval $G_{ox0} = 0.186-1.35$ kg/s. When the valves were opened for air displacing liquid oxygen, the air pressure decreased approximately by one third because air started to fill the input pipelines and the space of the flowmeter above the piston. The current flow rate of hydrogen was determined on the basis of the pressure decrease in the receiver $p_{r,f}$, and the current flow rate of oxygen was determined from the path covered by the piston L_p , which was detected by the rheostat 8 [4]. The specific flow rate of the mixture was

$g_{\Sigma} = (G_f + G_{ox})/S_{\Delta} = 20-230$ kg/(s · m²), and the fuel-to-oxidizer equivalence ratio was $\phi = (G_f/G_{ox})\chi_{st} = 0.6-2.9$. Here $S_{\Delta} = \pi d_{c1} \Delta$ is the area of the cylindrical surface of the plane-radial combustor at the entrance, and $\chi_{st} = 8$ is the stoichiometric coefficient. The process initiator 9 was placed in the plane wall at a distance of 20 mm from the combustor entrance. It contained an aluminum foil strip burned by electric current with the energy release approximately equal to 5 J. Initiator actuation was synchronized with oxygen injection into the combustor, which occurred later than hydrogen injection. The products escaped into the atmosphere with the ambient pressure $p_a = 1.0 \cdot 10^5$ Pa. The process was observed through two Plexiglas windows 10 (95 mm long and 10 mm wide), which were placed in one of the plane walls and covered almost the entire flow field along the window. Only a small flow region near the injectors at a distance of 5 mm could not be observed.

The process in the plane-radial combustor was photographed by the Photron Fastcam SA5 high-speed camera with a frequency of 700 000 fps. Processing of the frames by a special program provided photographic records of the flow in the wave-fitted system. As the photographic records had a linear form, the luminescent objects moving in the tangential direction were recorded with distortion because they moved over circumferences of different diameters. A special program was used to convert the flat photographic records into a ring. Based on the photographic records, we determined the time when the detonation waves appeared opposite to the windows Δt , which ensured unique determination of their frequency $f = 1/\Delta t$. In the CSD case, we also calculated the velocity of motion of transverse detonation waves (TDWs) D with respect to the cylindrical surface having the diameter d_{c1} : $D = \pi d_{c1}/(n\Delta t)$ (n is the number of TDWs over the combustor circumference).

We measured the mean current pressures in the hydrogen receivers $p_{r,f}$ and air receivers $p_{r,ox}$, the pressures in the corresponding manifolds ($p_{m,f}$ and $p_{m,ox}$), the static pressure in the combustor (p_{c1}) at a distance of 10 mm from the cylindrical surface of the plane-radial combustor (position 11), the static pressure (p_{c2}) and total pressure (p_{c20}) measured by the Pitot tubes at a distance of 50 mm from the cylindrical surface of the combustor (position 12), and the static and total pressures (p_{c3} and p_{c30} , respectively) at a distance of 100 mm from this surface (position 13). The sensors 12 and 13 measured the pressure at the exit from the combustors of lengths $L_c = 50$ and 100 mm, respectively. The pressures were measured by certified sensors with the class of accuracy 0.5%, which were produced by the Trafag company (Switzerland).

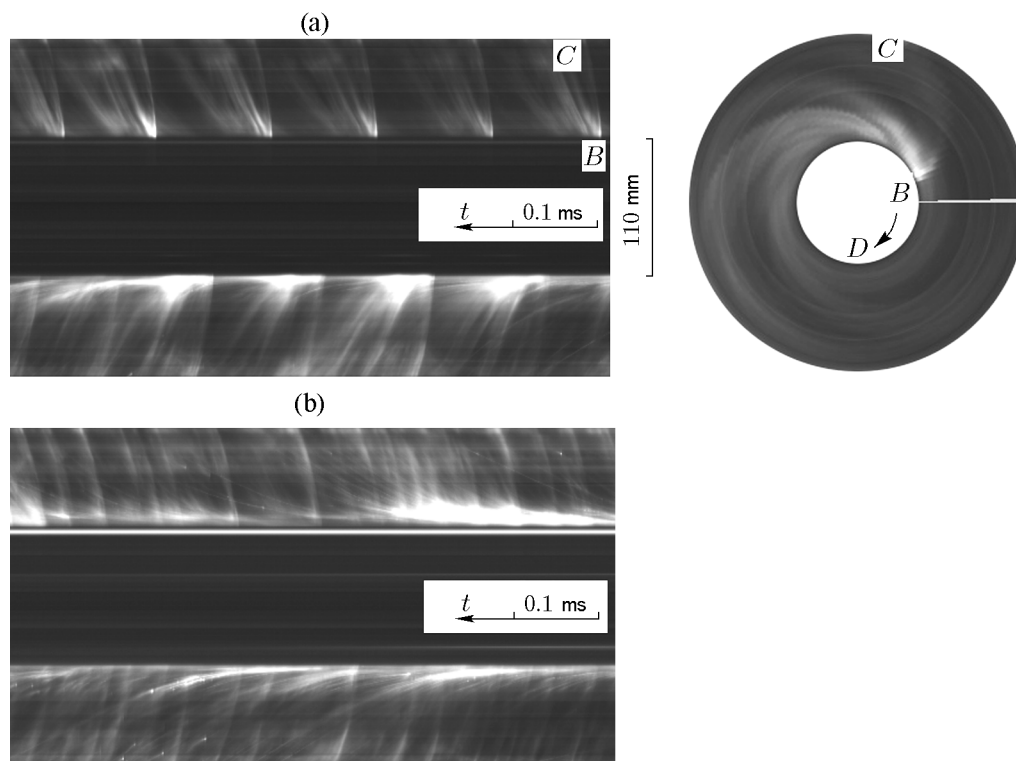


Fig. 2. Fragments of the photographic records of CSD and reconstruction of TDWs in the plane of the plane-radial combustor (a) and photographic records of CMD (b) in the combustor of length $L_c = 100$ mm for $\Delta = 10$ mm = const: (a) $g_\Sigma = 183$ kg/(s·m²), $\phi = 0.87$, $n = 1$, and $D = 2.66$ km/s ($f = 8.46$ kHz); (b) $g_\Sigma = 166$ kg/(s·m²), $\phi = 0.7$, and $f \approx 23$ kHz.

2. RESULTS OF EXPERIMENTS

2.1. Combustor with the Diameter $d_{c2} = 300$ mm

Plane-Radial Combustor with $\Delta = 10$ mm = const. Continuous spin detonation with one ($n = 1$) TDW was obtained in the ranges of the specific flow rates of the mixture $g_\Sigma = 180$ – 230 kg/(s·m²), equivalence ratios $\phi = 0.86$ – 1.29 , and combustor pressures $p_{c1} = (2.1$ – $3.2) \cdot 10^5$ Pa. With respect to the internal cylindrical surface of the combustor, this TDW moved with the velocities $D = 2.4$ – 3.58 km/s ($f = 7.64$ – 11.4 kHz). Figure 2a shows a fragment of the photographic records of CSD with one TDW and its reconstruction in the plane of the combustor.

The photographic records taken through the upper and lower windows (see position 10 in Fig. 1) are separated by a 110-mm dark band reflecting the space between the windows. The detonation front BC moves from left to right with a sufficiently high phase velocity D . The true velocity of the wave is determined by the normal to the front BC , which becomes more and more deflected backward as the combustor chan-

nel radius increases (there is no other explanation for the tripled velocities at the combustor periphery with the orifice diameter $d_{c2} = 300$ mm). The detonation wave front BC covers the entire length of the combustor $h \approx L_c = 100$ mm. The tail CD (shock wave adjacent to the front) extends outside the combustor; for this reason, it is not seen in the photographic records. The photographic records display identical directions of TDW motion in the upper and lower windows, though it is clear that the wave in these windows moves in the opposite directions. The true direction of the TDW can be determined by watching the movie. Based on the contrast of the wave image, we determined the direction of scanning of the object by the camera. If it coincided with the wave direction, the wave velocity was compensated to a certain extent, and the image contrast was greater (upper band); otherwise, the wave structure was smeared (lower band).

In the ranges $g_\Sigma = 151$ – 180 kg/(s·m²), $\phi = 0.6$ – 0.86 , and $p_{c1} = (1.6$ – $2.1) \cdot 10^5$ Pa, we observed the CMD regime with opposing TDWs (Fig. 2b). The process is rather irregular in terms of the TDW velocity and structure. It is difficult even to determine the

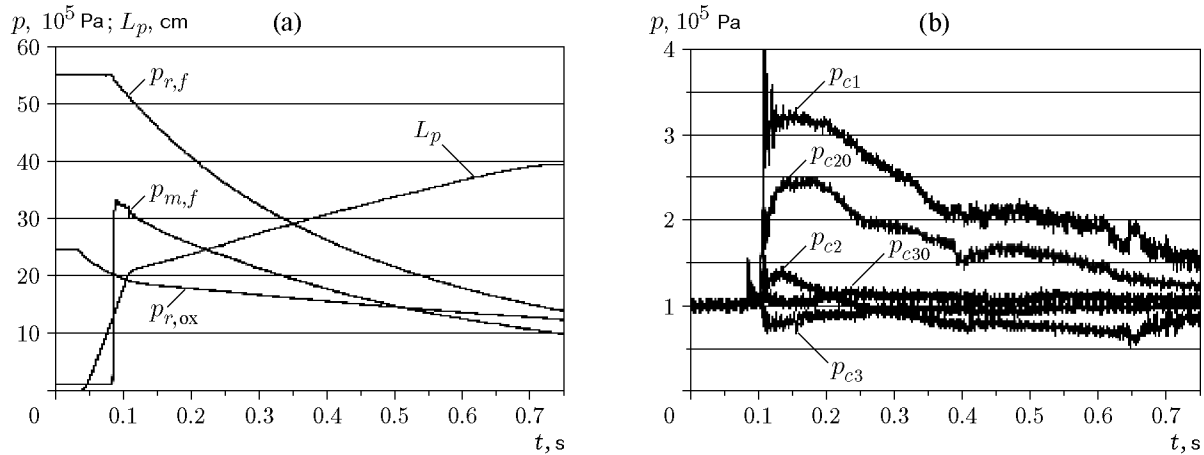


Fig. 3. Oscillograms of the pressure and piston path in the injection system (a) and in the combustor (b) for the combustor length $L_c = 100$ mm and $\Delta = 10$ mm = const.

number of TDWs, and it is impossible to understand their location in the combustor plane from the photographic records taken through the longitudinal windows 10. For this purpose, it is necessary to take individual frames through the entire transparent wall of the combustor, which was done, e.g., in the plane-radial combustor with exhaustion toward the center [6]. Figure 3 shows the oscillograms of the process whose photographic records are presented in Fig. 2.

The initial time t was taken to be the instant of actuation of the control valves of the injection system, initiation, and recording equipment. The first valve to be opened is the valve responsible for air injection with the pressure $p_{r,ox}$ to the piston of the flowmeter of liquid oxygen (see position 5 in Fig. 1). The membrane 7 is broken, and the piston starts to move (curve L_p). The drastic inflection on the curve L_p corresponds to complete displacement of air from the oxygen manifold 4 and filling of this manifold with liquid oxygen. The further path of the piston demonstrates the displacement of liquid oxygen to the combustor. The second inflection of the curve L_p corresponds to termination of piston motion at the lower point of the flowmeter 5, after which air starts to displace liquid oxygen still remaining in the manifold 4. The second valve that was opened was the valve of injection of hydrogen with the pressure $p_{r,f}$, which left the receiver. At the instant of initiation, the pressure in the combustor drastically increased (see Fig. 3b). As hydrogen exhausted from a finite volume $V_{r,f}$, its flow rate decreased during the experiment. At the same time, the piston displacing liquid oxygen from the flowmeter moved with an almost constant velocity. Therefore, both the equivalence ratio ($\phi = 1.55 \rightarrow 0.7$) and the pressure in the combustor decreased during the experiment. It follows from the ratios of the total and

static pressures in the middle of the combustor p_{c20}/p_{c2} and at the combustor exit p_{c30}/p_{c3} that exhaustion of the products from the combustor was subcritical, and the pressure jump reached the middle of the combustor only at the end of the experiment. The main parameters of the flow regime are listed in the first row of the table. Here $p_a \approx 1 \cdot 10^5$ Pa is the ambient pressure, and the arrows indicate the direction in which the parameters changed during the experiment. As the piston motion was nonuniform in some experiments, the parameters given in the table are outside the limits of the indicated minimum and maximum values.

Plane-Radial Combustor with $S_\Delta \approx \text{const.}$ For the combustor channel constriction from $\Delta = 10$ to $\Delta' = 3.3$ mm (see Fig. 1), conventional combustion was observed in the ranges $g_\Sigma = 90.9\text{--}93.4$ kg/(s·m²), $\phi = 2.9\text{--}4.38$, and $p_{c1} = (4.1\text{--}4.64) \cdot 10^5$ Pa, which was associated with instability of oxygen injection into the combustor. Figure 4a shows the scanned patterns of combustion product particles moving in the radial direction (x - t diagram). On the background of combustion, one can see weak acoustic waves moving in the tangential direction.

If oxygen injection into the combustor was stabilized ($t > 0.23$ s), the CSD regime was observed in the ranges $g_\Sigma = 20\text{--}122$ kg/(s·m²), $\phi = 1.09\text{--}2.9$, and $p_{c1} = (1.7\text{--}3.7) \cdot 10^5$ Pa. The mixture was burned in the front BC in a considerable number of TDWs ($n = 3\text{--}6$) whose velocities with respect to the internal cylindrical surface were $D = 2.42\text{--}2.86$ km/s ($f = 30.8\text{--}54.6$ kHz). Figure 4b shows a fragment of the photographic records for the CSD regime with five TDWs and their reconstruction in the combustor plane.

Figure 4c shows the pressure oscillograms inside the combustor. It is seen that the pressure in the com-

Parameters of the processes in the combustors with the lengths $L_c = 100$ and 50 mm

L_c , mm	g_Σ , kg/(s·m ²)	ϕ	f , kHz	n	D , km/s	p_{c1}/p_a	Regime
100 ($\Delta = 10$ mm)	230 → 180	1.29 → 0.87	11.2 → 8.46	1	3.56 → 2.65	3.1 → 2.1	CSD
	180 → 151	0.87 → 0.6	24.6 → 23	—	—	2.1 → 1.5	CMD
100 ($\Delta' = 3.3$ mm)	122 → 20	2.9 → 1.09	54.6 → 30.8	6 → 3	2.86 → 2.42	3.7 → 1.7	CSD
50 ($\Delta = 10$ mm)	165 → 128	1.88 → 1.8	9.91 → 9.24	1	3.11 → 2.9	3.8 → 2.2	CSD
	128 → 86	1.8 → 1.43	—	—	—	2.2 → 2.0	Unstable TDWs
	86 → 83	1.43 → 1.0	24 → 19.9	3 → 4	2.55 → 1.56	2.0 → 1.8	CSD
50 ($\Delta' = 5$ mm)	284 → 136	0.99 → 1.03	—	—	—	6.1 → 2.5	Combustion
	136 → 82	1.03 → 0.9	83.3 → 48.2	10 → 7	2.61 → 2.16	2.3 → 1.52	CSD

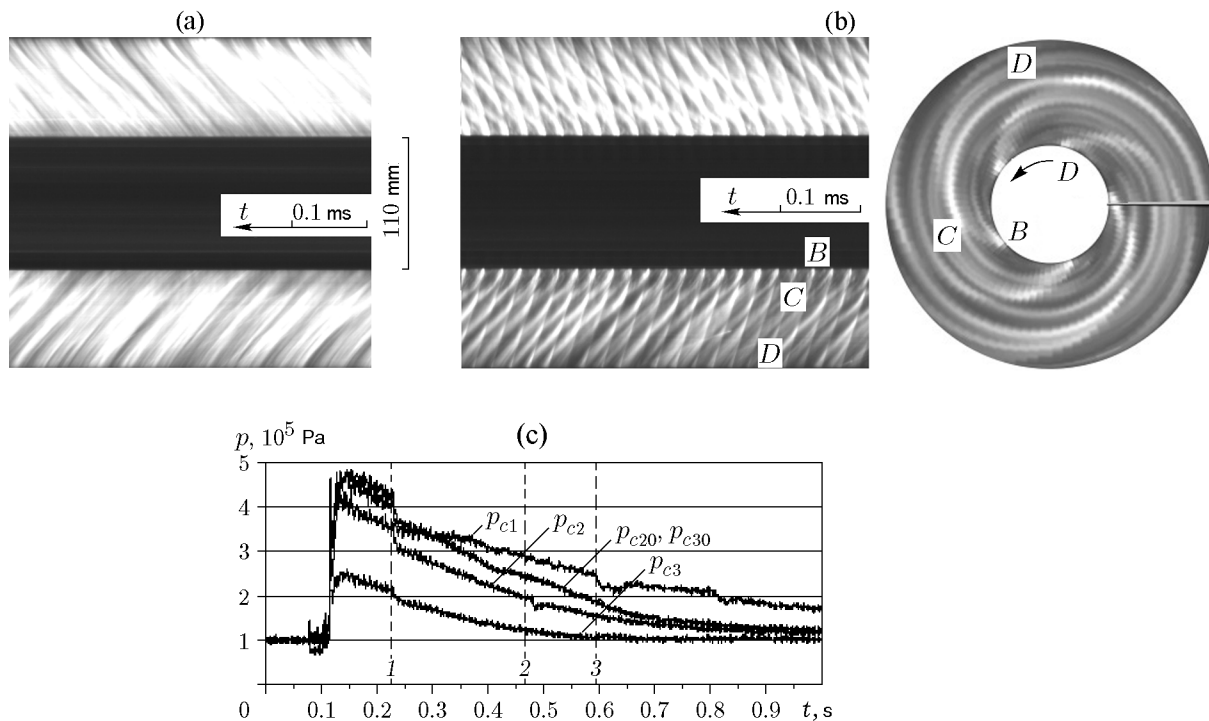


Fig. 4. Fragments of the photographic records (a and b) and pressure oscillograms (c) for the plane-radial combustor with the length $L_c = 100$ mm and $S_\Delta \approx \text{const}$: (a) combustion, $g_\Sigma = 93$ kg/(s·m²) and $\phi = 3$; (b) CSD process and reconstruction of TDWs in the combustor plane, $g_\Sigma = 116$ kg/(s·m²) and $\phi = 1.33$, $n = 5$, and $D = 2.614$ km/s ($f = 41.6$ kHz); the instants corresponding to combustion (a), CSD (b), and beginning of subcritical exhaustion from the combustor are marked by 1, 2, and 3, respectively.

bustor is appreciably higher than that in the experiment with $\Delta = 10$ mm = const (see Fig. 3b). However, the values of the total pressures in the middle of the combustor and at the combustor exit almost coincide: $p_{c20} \approx p_{c30}$. The jump-like change in the combustor pressure ($t \approx 0.23$ s) is related to unstable injection of liquid oxygen caused by the length covered by the flowmeter piston L_p . The test results are listed in the table. However, because of the nonuniform mo-

tion of the piston displacing oxygen from the flowmeter, there were jumps of the specific flow rate of the mixture within $\pm 5\%$, which did not produce any noticeable effect on the CSD regime.

2.2. Combustor with the Diameter $d_{c2} = 200$ mm

Plane-Radial Combustor with $\Delta = 10$ mm = const.
In the ranges $g_\Sigma = 128$ – 165 kg/(s·m²), $\phi = 1.8$ – 1.88 ,

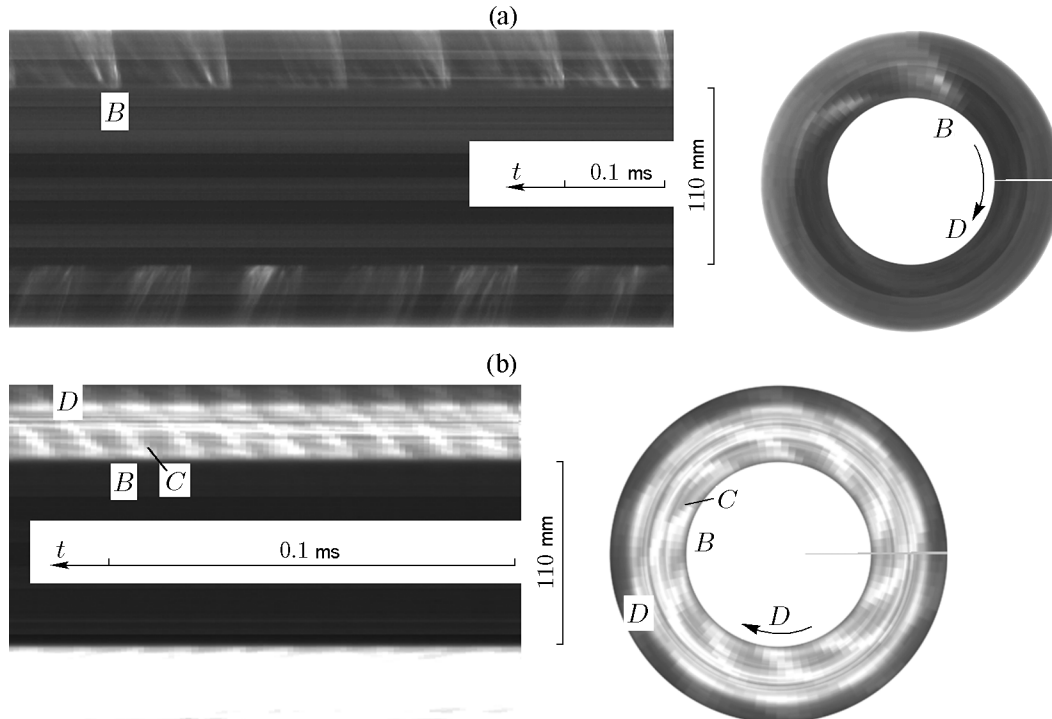


Fig. 5. Fragments of the photographic records and reconstruction of TDWs in the plane-radial combustor with the length $L_c = 50$ mm: (a) $\Delta = 10$ mm = const, $g_\Sigma = 168$ kg/(s·m²), $\phi = 1.56$, $n = 1$, and $D = 2.93$ km/s ($f = 9.32$ kHz); (b) $S_\Delta \approx$ const, $g_\Sigma = 135$ kg/(s·m²), $\phi = 1.04$, $n = 10$, and $D = 2.61$ km/s ($f = 83.3$ kHz).

and $p_{c1} = (2.2\text{--}3.8) \cdot 10^5$ Pa, a stable CSD regime with one TDW was observed (Fig. 5a). In addition to the fragment of the photographic records, Fig. 5 (on the right) shows the TDW location and the flow in its vicinity in the combustor plane. The combustor length $L_c = 50$ mm turned out to be insufficient for the mixture formed in the combustor to be burned in the detonation wave. Therefore, Fig. 5a shows only the upper point of the wave B , whereas the lower point C and the tail CD are outside the combustor. With respect to the internal cylindrical surface, the TDW moved with the velocities $D = 2.9\text{--}3.11$ km/s ($f = 9.24\text{--}9.91$ kHz). In the ranges $g_\Sigma = 86\text{--}128$ kg/(s·m²), $\phi = 1.43\text{--}1.8$, and $p_{c1} = (2.0\text{--}2.2) \cdot 10^5$ Pa, the CSD regime became unstable, the TDWs became irregular, and the number of TDWs varied ($n = 2 \leftrightarrow 4$). The flow regime recovered its regularity at $g_\Sigma = 83\text{--}86$ kg/(s·m²), $\phi = 1.0\text{--}1.43$, and $p_{c1} = (1.8\text{--}2.0) \cdot 10^5$ Pa. First the regime with three TDWs rotating with the velocity $D = 2.32\text{--}2.55$ km/s ($f = 22.2\text{--}24.0$ kHz) was formed, and then it transformed to the regime with four TDWs whose velocities were in the interval $D = 1.56\text{--}1.624$ km/s (see the third row in the table).

Plane-Radial Combustor with $S_\Delta \approx$ const. If the combustor channel constricted from $\Delta = 10$ to

$\Delta' = 5$ mm (see Fig. 1), conventional combustion similar to that on the photographic records shown in Fig. 4a was observed in the ranges $g_\Sigma = 136\text{--}284$ kg/(s·m²), $\phi = 0.99\text{--}1.03$, and $p_{c1} = (2.5\text{--}6.1) \cdot 10^5$ Pa. This combustion transformed to the CSD regime with a large number of TDWs ($n = 10 \rightarrow 7$) at $g_\Sigma = 82\text{--}136$ kg/(s·m²), $\phi = 0.9\text{--}1.03$, and $p_{c1} = (1.55\text{--}2.3) \cdot 10^5$ Pa (see the fourth row in the table). A fragment of the photographic records including TDWs rotating in the combustor plane is shown in Fig. 5b (on the left), and the picture on the right is the reconstruction of the process to a ring-shaped structure. Here the point C , which denotes the lower edge of the detonation front BC , is outside the annular gap of the combustor.

3. ANALYSIS OF RESULTS

In the plane-radial combustor with exhaustion toward the periphery, detonation burning of mixtures of gaseous hydrogen and liquid oxygen was obtained for the first time in both CSD and CMD regimes. These regimes were obtained in this combustor in the case of burning of gaseous hydrogen-gaseous

oxygen mixtures [8, 9]. As the detonation front BC is curved and is significantly deflected toward the motion of the initial mixture (in the wave-fitted system), we chose its projection onto the combustor radius denoted by h for our analysis. In the plane–radial combustor of length $L_c = 100$ mm with $\Delta = 10$ mm = const, we obtained $h \approx L_c = 100$ mm and $h/l \approx 1/3$, where l is the distance between the neighboring TDWs (for $n = 1$, this is the length of the circumference of the internal cylindrical surface of the combustor). In the plane–radial combustor with $L_c = 50$ mm, less than one half of the incoming fresh mixture passed into the TDW front inside the annular channel. Naturally, for obtaining the optimal regime of CSD in the above-mentioned ranges of the specific flow rates of the mixture, the channel length should be increased at least to $(2 - 2.5)h$ ($L_{c,\min} = 200$ and 250 mm).

In the plane–radial combustors of lengths $L_c = 100$ and 50 mm with $S_\Delta \approx \text{const}$, the heights of the front BC for the above-mentioned ranges of the specific flow rates are $h \approx 25$ mm ($h/l \approx 1/2.5$) and $h \approx 10$ mm ($h/l \approx 1/3$), respectively. Then, these combustors can be reduced by 2–3 times under the condition $L_{c,\min} = (2 - 2.5)h$. There is still an open question: Why does not the number of TDWs in these combustors differ by a factor of 2 despite similar flow rates of the mixtures? A small difference in the equivalence ratio is not expected to produce a significant effect on the number of waves. In the plane–radial combustor with $S_\Delta \approx \text{const}$ and $L_c = 100$ mm, the mixture of gaseous hydrogen and gaseous oxygen with $g_\Sigma = 116$ kg/(s·m²) and $\phi \approx 1.0$ also burned in five TDWs, but their velocity and frequency were much smaller: $D = 2.06$ km/s and $f = 32.8$ kHz [9]. The detonation front height was $h \approx 15$ mm, and $h/l \approx 1/4$. The smaller height of the TDW front in the case of gas detonation was caused by a thinner critical layer of the mixture for detonation as compared to the gas–droplet mixture of these components. In the annular cylindrical combustor with the diameter $d_c = 100$ mm and surface area at the entrance $S_\Delta \approx \text{const}$, three waves moving with the velocity $D = 2.42$ km/s ($f = 23.1$ kHz) were observed in the case of CSD of the mixture of gaseous hydrogen and liquid oxygen with similar specific flow rates [4]. However, the front height was $h \approx 10$ mm, and $h/l \approx 1/10$. A smaller front height as compared to its value in the plane–radial combustor was caused by the fact that the centrifugal forces acting along the combustor channel did not affect the products.

As it could be expected, the real flow rates of oxygen in the case of an unsteady thermal regime of exhaustion of the cryogenic liquid turned out to be smaller than the values predicted with ignored influence of evapora-

tion in the injection path including the pipeline downstream from the membrane 7, manifold 4, and injectors 2 (see Fig. 1). Obviously, the fraction of gaseous oxygen increases with increasing time of the contact of the liquid phase with the injection path surface and also with increasing area of this surface. Indeed, for higher pressures of oxygen injection, this time decreased and the output of the liquid phase of oxygen increased. For example, the oxygen flow rate was $G_{\text{ox}} = 1.35$ kg/s for the air pressure $p_{r,\text{ox}} = 37 \cdot 10^5$ Pa and $G_{\text{ox}} = 0.51$ kg/s for $p_{r,\text{ox}} = 18 \cdot 10^5$ Pa. Using the estimate of the flow rate of oxygen by the formula $G_{\text{ox}} = \mu \rho_{\text{ox}} v_{\text{ox}} S_{\text{ox}}$ with oxygen evaporation being ignored, we obtain $G_{\text{ox}} = 2.18$ and 1.53 kg/s, which is greater than the true flow rates by a factor of 1.61 and 3, respectively. Here $\mu = 0.875$ is the flow rate coefficient in the injection channels with sharp inputs [11], $\rho_{\text{ox}} = 1.2 \cdot 10^3$ kg/m³ is the density of liquid oxygen at the nitrogen boiling point $T_h = 77$ K [12], and $v_{\text{ox}} = (2\Delta p / \rho_{\text{ox}})^{0.5}$ is the velocity of oxygen exhaustion for the pressure difference at the injector orifices $\Delta p = p_{m,\text{ox}} - p_{\text{st}}$, where p_{st} is the static pressure in the combustor at the injector exits. It should be noted that we failed to measure the pressure in the oxygen manifold $p_{m,\text{ox}}$ precisely because liquid oxygen entering the tube connected to the sensor started to evaporate, and the sensor readings were greater than the pressure of displacing air in the receiver $p_{r,\text{ox}}$. In the case of exhaustion of gaseous oxygen through the injector orifices, the pressure in the manifold differed from the pressure in the receiver by less than 10% [8, 9]. As the cross-sectional area of the orifices of the injector for liquid oxygen was twice smaller than the cross-sectional area of the orifices of the injector for the gas and the velocity of exhaustion of the liquid phase was approximately five times smaller at the injection pressure $p_{r,\text{ox}} = 25 \cdot 10^5$ Pa ($v_{\text{ox}} \approx 60$ m/s), we can argue that the error of determining the liquid phase velocity under the assumption that $p_{m,\text{ox}} \approx p_{r,\text{ox}}$ did not exceed 2.5%. The difference in the static pressures at the injector exit and at a distance of 10 mm can be neglected because it is within $1 \cdot 10^5$ Pa (see Figs. 3 and 4). If an obstacle (M16 nut) was placed into the oxygen injection path, the area of the contact of liquid oxygen with the metal with an initial room temperature increased, thus, increasing the fraction of the gas phase.

Let us estimate the possibility of heating liquid oxygen from the walls of the injection path. The characteristic thickness of cooling of the injection path walls δ_w is estimated as $\delta_w = (a_w t)^{0.5}$, where $a_w = \lambda_w / (\rho_w c_w)$ is the thermal diffusivity of the wall material, whereas λ_w , ρ_w , and c_w are its thermal conductivity, density, and specific heat, respectively. To estimate the temperature, we use the mean values of the constants in the tempera-

ture interval from T_{0w} to T_h , where $T_{0w} = 296$ K is the initial temperature of the oxygen injection path walls, and T_h is the oxygen boiling temperature corresponding to the pressure $p_{r,ox}$. Let us consider only one example where the oxygen boiling point in the injection path with the wall area $S_w = 250$ cm² at the oxygen injection pressure $p_{r,ox} = 30 \cdot 10^5$ Pa is $T_h = 141.5$ K. The mean values of the constants for stainless steel [10] are $\lambda_w = \langle \lambda_w \rangle \approx 28.8$ J/(m·s·K), $\rho_w = \langle \rho_w \rangle \approx 8 \cdot 10^3$ kg/m³, and $c_w = \langle c_w \rangle \approx 376$ J/(kg·K). Then, $a_w = 9.57 \cdot 10^{-6}$ m²/s, and we obtain $\delta_w = 2.4$ mm during the exhaustion time $t = 0.6$ s. The heat Q_w transferred from the injection path walls is estimated as $Q_w = m_w c_w (T_{0w} - T_h) = \rho_w S_w \delta_w c_w (T_{0w} - T_h) = 47.5$ kJ. This amount of heat is sufficient to heat the oxygen mass $m_{ox} = Q_w / [J_h + (J_{ox(liq)2} - J_{ox(liq)1})] \approx 0.1$ kg to the boiling point. Here $J_h = 378$ kJ/kg is the heat of evaporation at the boiling temperature $T_h = 141.5$ K; $J_{ox(liq)1} = -155$ kJ/kg and $J_{ox(liq)2} = -24$ kJ/kg are the enthalpies of liquid oxygen at $T_{0ox} = 77$ K and $T_h = 141.5$ K, respectively. Approximately 0.5 kg of liquid oxygen were usually poured into the flowmeter; therefore, its gasification with the vapor density $\rho_{ox,h} \approx 0.1 \cdot 10^3$ kg/m³ at $T_h = 141.5$ K could possibly reduce the predicted flow rates of oxygen by a factor of 3 and more.

It was noted that the piston velocities (oxygen flow rates G_{ox}) were often different for identical injection pressures $p_{r,ox}$, especially for their low values. This is apparently related to the formation of the primary detonation wave in the plane–radial combustor propagating from the initiation point over the fuel mixture filling the combustor. In this case, the products were inevitably ejected into the oxygen manifold, and some part of oxygen evaporated due to the contact with the products. The velocity of oxygen exhaustion decreased, and the liquid column in the flowmeter sometimes started to move in the opposite direction. The contact time of oxygen with the walls increased, resulting in additional gasification. As a result, the regime of exhaustion of a gas–liquid oxygen system was formed, depending on the initial degree of the influence of the primary detonation wave on the injection system.

Continuous detonation was always formed in the plane–radial combustor with $\Delta = 10$ mm = const in the above-mentioned ranges of the specific flow rates of the mixture: CSD or CMD in the combustor with $L_c = 100$ mm and only CSD in the combustor with $L_c = 50$ mm. Moreover, the CMD regime was observed in the combustor with $L_c = 100$ mm almost in the same range of the flow rates $g_\Sigma = 151$ – 180 kg/(s·m²) as that in the experiments with gaseous hydrogen and gaseous oxygen [8, 9]. Thus, the governing factor for this com-

bustor is the combustor geometry, while mixing plays a secondary role. Constriction of the combustor gap to $\Delta' = 3.3$ mm ($S_\Delta \approx$ const) resulted in the formation of the CSD regime (as in [8, 9]). The combustion observed at the beginning of the experiment may be caused by oscillations of the piston of the flowmeter around its initial position and by the off-design regime of oxygen displacement into the combustor. The types of flow regimes at high specific flow rates of the fuel $g_\Sigma > 122$ kg/(s·m²) have not been yet clarified. Apparently, there was the same regime of combustion that was observed in the combustor with $L_c = 50$ mm and channel constriction.

An important issue for obtaining the CSD regime in the combustor with $L_c = 50$ mm and $\Delta = 10$ mm = const is the degree of mixing along the combustor because one half of the mixture is ejected outward and burns there in the detonation wave outside the combustor. For some reason, conditions for CMD existence are not formed there. In the case of gaseous components [8, 9], the detonation front occupies approximately one third of the combustor length [$h \approx (1/3)L_c$]; therefore, the conditions formed there could ensure both the CSD and CMD regimes. Conventional combustion was observed at $\Delta' = 5$ mm ($S_\Delta \approx$ const) and $g_\Sigma > 136$ kg/(s·m²), though the ratio of the species was fairly favorable. It was only at $g_\Sigma < 136$ kg/(s·m²) that the transition to CSD occurred; moreover, the CSD regime had a large number of TDWs ($n = 10$) and a small front height ($h \approx 10$ mm). Comparing the estimated (with the vapor phase being ignored) and real flow rates of oxygen, we found that CSD was observed if the fraction of the gaseous oxygen phase was greater than 70%. For smaller fractions of gaseous oxygen, the hydrogen jets do not have enough time to split the oxygen jets and droplets within the distance $h \approx 10$ mm from the injectors, and the resultant mixture starts burning in the conventional combustion regime. If the fraction of gaseous oxygen is greater than 70%, a detonation-capable layer of the mixture of gaseous oxygen and gaseous hydrogen is formed and CSD occurs with fragmentation of the remaining oxygen droplets and burning of the remaining hydrogen in the fronts of the CSD process. For this reason, it is reasonable to inject oxygen in the supercritical state into the combustor; in this case, the entire amount of oxygen transforms to the gas phase when it enters a high-temperature medium and the pressure is released. At $\Delta = 10$ mm = const, the combustible mixture was formed in the combustor region with an expanding area, and the flame was not held near the injectors; therefore, the detonation-capable layer was formed at a greater distance from the injectors without burnout ahead of the detonation wave front.

CONCLUSIONS

1. Regimes of continuous spin detonation and continuous multifront detonation in the gas–droplet mixture of gaseous hydrogen and liquid oxygen were obtained for the first time in a plane–radial combustor (with the internal and external diameters equal to 100 and 300 mm, respectively) with exhaustion toward the periphery. Regimes of continuous spin detonation were obtained in the combustor with the external diameter of 200 mm.

2. The structure of detonation waves was considered. For the CSD regime, reconstruction of transverse detonation waves and the flow in their vicinity in the plane of the combustor was performed. It was demonstrated that the detonation wave is significantly curved because of the increase in the tangential component of velocity along the combustor radius.

3. It was shown that the height of the detonation-capable layer of the mixture in the plane–radial combustor with exhaustion toward the periphery increases owing to the presence of centrifugal forces acting on the products in the detonation wave front and also in the expansion wave. As a result, the ratio of the height of this layer to the distance between the neighboring transverse detonation waves decreases.

4. The fraction of gaseous oxygen after the oxidizer flow passed through the injection system was estimated. It was demonstrated by an example of the combustor with the external diameter of 200 mm and constriction at the exit that continuous spin detonation is formed if the fraction of the gas phase in the oxygen flow is greater than 70%.

This work was supported by the Russian Foundation for Basic Research (Grant No. 18-41-540001r.a).

REFERENCES

1. B. V. Voitsekhovskii, “Steady Detonation,” *Dokl. Akad. Nauk SSSR* **129** (6), 1254–1256 (1959).
2. F. A. Bykovskii, A. A. Vasil’ev, E. F. Vedernikov, and V. V. Mitrofanov, “Explosive Combustion of a Gas Mixture in Radial Annular Chambers,” *Fiz. Goreniya Vzryva* **30** (4), 111–118 (1994) [*Combust., Expl., Shock Waves* **30** (4), 510–516 (1994)].
3. F. A. Bykovskii and E. F. Vedernikov, “Self-Sustaining Pulsating Detonation of Gas-Mixture Flow,” *Fiz. Goreniya Vzryva* **32** (4), 99–106 (1996) [*Combust., Expl., Shock Waves* **32** (4), 442–448 (1996)].
4. F. A. Bykovskii and S. A. Zhdan, *Continuous Spin Detonation* (Izd. Sib. Otd. Ross. Akad. Nauk, Novosibirsk, 2013) [in Russian].
5. F. A. Bykovskii, S. A. Zhdan, E. F. Vedernikov, et al., “Continuous Detonation of a Hydrogen–Oxygen Mixture in a Plane–Radial Combustor with Exhaustion toward the Periphery,” in *Proc. XXXI Siberian Thermophysical Workshop, November 17–19, 2014, Novosibirsk, Russia*, pp. 173–178.
6. J. Higashi, C. Ishiyama, S. Nakagami, et al., “Experimental Study of Disk-Shaped Rotating Detonation Turbine Engine,” in *Proc. 55th AIAA Aerospace Sciences Meeting* (2017); <https://doi.org/10.2514/6.2017-1286>.
7. F. A. Bykovskii, S. A. Zhdan, E. F. Vedernikov, et al., “Detonation of a Hydrogen–Oxygen Gas Mixture in a Plane–Radial Combustor with Exhaustion Toward the Periphery in the Regime of Oxygen Ejection,” *J. Phys: Conf. Ser.* **1128**, 012075 (2018).
8. F. A. Bykovskii, S. A. Zhdan, E. F. Vedernikov, et al., “Continuous Detonation of a Hydrogen–Oxygen Gas Mixture in a Plane–Radial Combustor with Exhaustion Toward the Periphery,” in *Advances in Pulsed and Continuous Detonations*, Ed. by S. M. Frolov (Torus press, Moscow, 2019), pp. 309–324.
9. F. A. Bykovskii, S. A. Zhdan, E. F. Vedernikov, et al., “Continuous Detonation of a Hydrogen–Oxygen Gas Mixture in a 100-mm Plane–Radial Combustor with Exhaustion Toward the Periphery,” *Shock Waves* **30** (3), 235–243 (2020); <https://doi.org/10.1007/s00193-019-00919x>.
10. *Physical Quantities: Reference Book*, Ed. by I. S. Grigor’ev and E. Z. Meilikhov (Energoatomizdat, Moscow, 1991) [in Russian].
11. F. A. Bykovskii and E. F. Vedernikov, “Discharge Coefficients of Nozzles and of Their Combinations in Forward and Reverse Flow,” *Prikl. Mekh. Tekh. Fiz.* **37** (4), 98–104 (1996) [*J. Appl. Mech. Tech. Phys.* **37** (4), 541–546 (1996)].
12. N. V. Vargaftik, *Reference Book on Thermophysical Properties of Gases and Liquids* (Nauka, Moscow, 1977) [in Russian].